Journal of The Electrochemical Society, **158** (11) H1161-H1165 (2011)
0013-4651/2011/158(11)/H1161/5/$28.00 © The Electrochemical Society

Thermal Stability and Performance of NbSiTaTiZr High-Entropy Alloy Barrier for Copper Metallization

Ming-Hung Tsai,[a,b] Chun-Wen Wang,[c] Che-Wei Tsai,[a] Wan-Jui Shen,[a] Jien-Wei Yeh,[a,z] Jon-Yiew Gan,[a] and Wen-Wei Wu[c]

[a]*Department of Materials Science and Engineering, National Tsing Hua University, Hsinchu 30013, Taiwan*
[b]*Department of Materials Science and Engineering, North Carolina State University, Raleigh, North Carolina 27695, USA*
[c]*Department of Materials Science and Engineering, National Chao Tung University, Hsinchu 30010, Taiwan*

Development of better diffusion barriers for Cu metallization is one of the key issues for the microelectronics industry. Although metallic diffusion barriers offer many advantages, their application is hindered due to their inferior thermal stability relative to ceramic barriers. Here we report on a metallic diffusion barrier, NbSiTaTiZr, which shows thermal stability comparable to ceramic barriers. The outstanding performance of NbSiTaTiZr is due to its better structural and chemical stability at high temperatures.
 [DOI: 10.1149/2.056111jes]

Manuscript submitted June 10, 2011; revised manuscript received August 15, 2011. Published October 5, 2011.

One of the major challenges in the miniaturization of modern microelectronic devices is the development of future diffusion barrier materials against the diffusion of Cu.[1] This is because Cu is known to be a fast diffuser in Si and SiO_2.[2,3] The invasion of Cu leads to numerous adverse effects, including the formation of deep trap levels that cause serious device degradation and failure. Cu Refractory metals have been considered as possible candidates for diffusion barrier for a long time.[4] Recently, metallic barriers have become even more attractive because they offer important advantages at extremely small feature sizes. For example, metal barriers offer lower resistivity, better adhesion to Cu (and thus better electromigration resistance),[5–7] and the possibility to electroplate Cu directly.[8–10]

However, most studies on new barrier materials still focus on ceramic barriers. This is because the failure temperature of metallic barriers (typically around 550–650°C) is apparently lower than that of ceramic ones (typically around 700–800°C). Metal barriers fail at lower temperature due to two main reasons: (1) the diffusion of Cu through barrier grain boundaries; or (2) reaction between barrier metal and Si. The first reason, namely the grain-boundary-assisted diffusion of Cu, is known to be the primary cause of barrier failure.[2] In ceramic barriers, the problem can be alleviated by using amorphous ceramics that do not contain grain boundaries; TaSiN is a classic example.[11] However, in the case of metallic barriers, this strategy is not effective because amorphous metal barriers crystallize below 550–650°C.[12,13] Therefore, the low *structural* stability of metals renders them ineffective in preventing the diffusion of Cu. The second problem of metallic barriers, on the other hand, comes from their low *chemical* stability. At around 550∼650°C, metals [even those with an extremely high melting point, such as W (3407°C), Ta (2996°C), and Mo (2617°C)] start to react with Si.[14–17] The reacted region continues to expand into the barrier until it completely consumes the barrier metal and reaches the other side. Since either of the two stability problems can lead to barrier failure, they need to be addressed *simultaneously* if one wants to improve the performance of metallic barriers. That is, the barrier has to maintain its amorphous structure and its inertness to Cu and Si to temperatures higher than 650°C.

Recently a new group of materials, so called "high-entropy alloys" (HEAs), has been developed.[18,19] These multi-principal-element alloys in general develop amorphous structure easily,[19–22] have good thermal stability,[23] and are chemically stable.[24] HEAs and their nitrides have been tested for diffusion barrier applications very recently. HEA nitrides showed excellent properties,[25–27] HEA barriers also showed improved performance depending on composition. For example, AlMoNbSiTaTiVZr and AlCrTaTiZr barriers were reported to fail at 750°C and 700°C,[28,29] respectively. AlCrRuTaTiZr was reported to remain effective until 800°C, although crystallization and reaction took place.[29] It is, therefore, possible that suitably-designed HEAs can offer a solution to the two stability problems of metal barriers. We have recently designed a new HEA, NbSiTaTiZr, with enhanced stability of amorphous structure. It is known that upon ten-minute annealing at 900°C this alloy sustains its amorphous structure.[30] Therefore, this alloy is potentially an excellent smetal diffusion barrier. In this paper we investigate the diffusion barrier properties of NbSiTaTiZr, and the mechanism of its structural and chemical stability. The mechanism could be also applied to assess other HEA diffusion barriers.

Experimental

Standard Cu(300 nm)/NbSiTaTiZr(20 nm)/Si test structures were fabricated to test the performance of the HEA as copper diffusion barrier. Although such test structure is used very often in the literature, it should be noted that in real devices, the diffusion barrier typically goes between Cu interconnect lines and some sort of dielectric, not between Cu and Si. NbSiTaTiZr and Cu films were sequentially deposited on (100) Si substrate by magnetron sputtering without breaking vacuum. Base pressure of the sputtering system was 8×10^{-6} Torr. Both depositions were conducted using Ar as working gas, at a fixed chamber pressure of 5 mTorr. Alloy barriers were sputtered with a dc power of 150 W and Cu films with an rf power of 80 W. Targets were presputtered before deposition to avoid contaminations. The NbSiTaTiZr alloy target used for sputtering was prepared via arc-melting the elemental raw materials (with purities better than 99.9%) in a vacuum chamber with a Ti-getter. The melting procedure was repeated five times to ensure that the constituents were completely mixed in the water-cooled copper crucible. The as-solidified round slab was then machined to a disk 2 inches in diameter and used as a sputtering target.

As-deposited samples were subsequently annealed between 650°C and 850°C for 30 minutes in a rapid thermal annealing furnace (RTA) at a pressure below 5×10^{-7} Torr. Grazing-incidence X-ray diffractions (GIXRD) were performed using an incidence angle of one degree and a scanning speed at four degrees per minute. Sheet resistances of the test structures and resistivity of the barrier were measured by four-point-probe method. Resistivity of the barrier was measured on a 20-nm-thick NbSiTaTiZr film deposited on thermally grown SiO_2 (200 nm)/Si substrate. Concentration profiles along the depth direction were analyzed by Auger electron spectroscopy (AES). Surface morphologies were observed with a field emission scanning electron microscope (FESEM) and interface reactions were investigated with high-resolution transmission electron microscopy (HRTEM). To determine the composition of the barrier layer, NbSiTaTiZr film with thickness around one micrometer was deposited on (100) Si wafer and examined via an electron probe x-ray microanalyzer (EPMA) so

[z] E-mail: jwyeh@mx.nthu.edu.tw

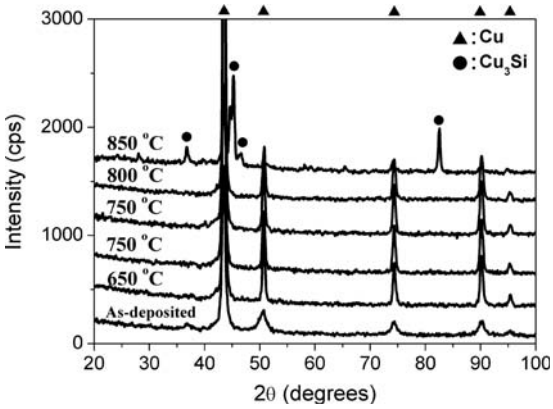

Figure 1. GIXRD patterns of the Cu/NbSiTaTiZr/Si test structure before and after annealing at various temperatures.

as to avoid substrate signals. The results show that the deviation from the desired equimolar composition is less than 1.5 at.%.

Results

The resistivity of the 20-nm-thick NbSiTaTiZr barrier was measured to be 205 μm cm, which is reasonably low. X-ray diffraction pattern of as-deposited test structure (Fig. 1) exhibits only peaks associated with Cu. No additional peaks can be observed up to an annealing temperature of 800°C for 30 min. At 850°C, however, peaks related to Cu_3Si appear, indicating the failure of the HEA barrier. The corresponding sheet resistances of the annealed samples (Fig. 2) are also seen to remain unchanged up to 800°C. Nevertheless, an abrupt increase in the sheet resistance occurs at 850°C. This is in agreement with silicide formation at this temperature, as noted from the GIXRD patterns.

The surface morphologies of test structures annealed at 800°C (before failure) and 850°C (failed) are shown in Fig. 3 . The surfaces of the 800°C-annealed samples are uniform and there is little contrast visible, as shown in Fig. 3a. High magnification image (inset of Fig. 3a) reveals coarsened Cu grains due to annealing. In contrast, a large number of square-shaped objects are observed on samples annealed at 850°C (Fig. 3b). Side-view of these objects (Fig. 3c) shows that they are actually inverted pyramid shaped – a typical shape of Cu_3Si. Indeed, EDS results reveal that these squares contain approximately 40 at.% Si and 60 at.% Cu, which clearly reveals that they are the sources of the silicide peaks in the XRD patterns of the 850°C-annealed samples. Some extraordinarily large Cu_3Si squares are surrounded by a circular zone (marked as A in Fig. 3b) within which the Cu film is depleted to form the central copper silicide. Outside these circular zones are the remnants of the Cu film (marked as B in Fig. 3b). A magnified view of the remnant Cu film is shown in the inset of Fig. 3b. Compared to the Cu film annealed at 800°C that shows only grains of Cu, dark zones about 50–150 nm in size appear on the remnant Cu film after annealing at 850°C. This suggests that barrier

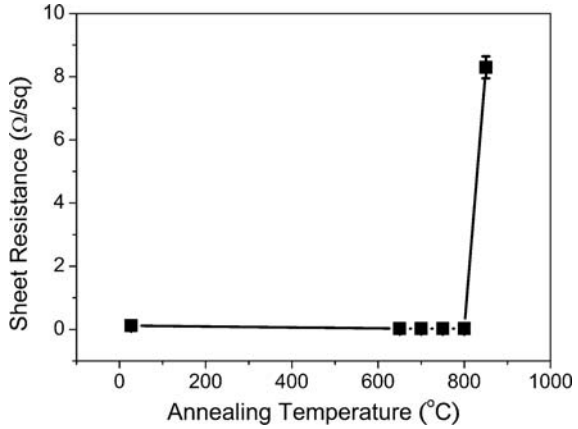

Figure 2. Sheet resistance as a function of annealing temperature for the Cu/NbSiTaTiZr/Si test structure.

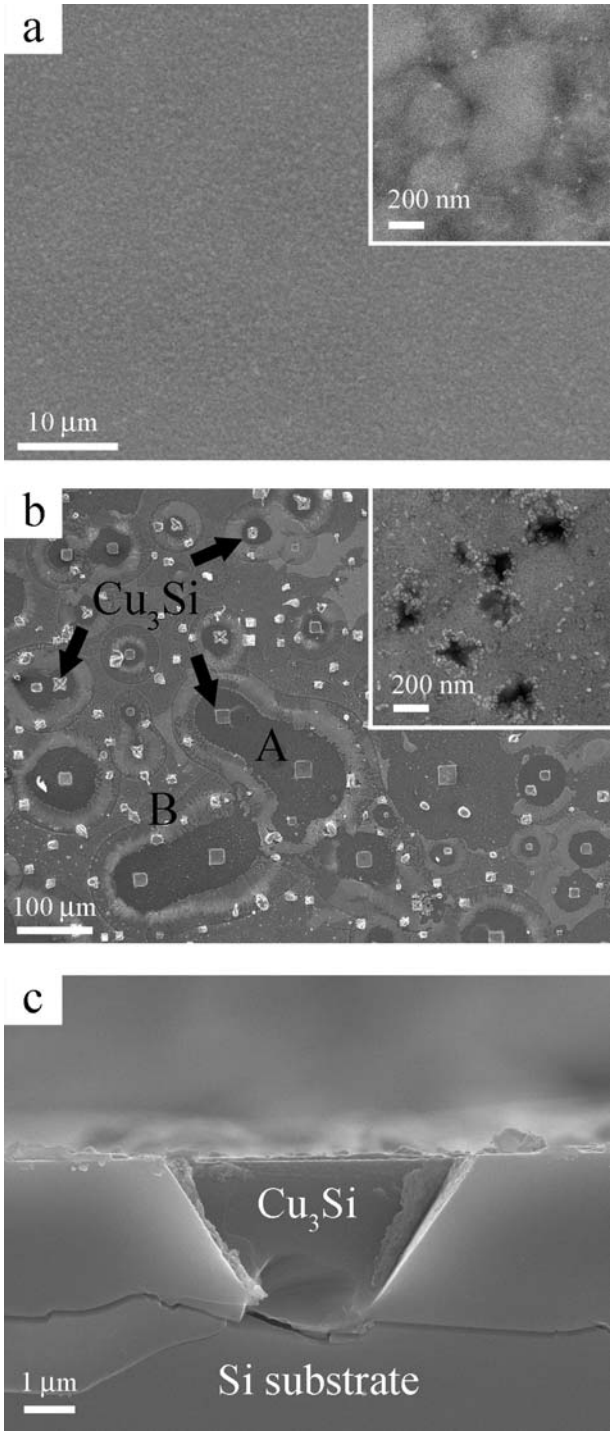

Figure 3. SEM micrographs of the test structure after annealing 30 min at (a) 800°C, and (b) 850°C. (c) Cross-sectional SEM image showing a typical inverted pyramid shaped Cu_3Si crystal embedded in the Si substrate of an 850°C-annealed test structure. Insets show higher magnification images of the copper film.

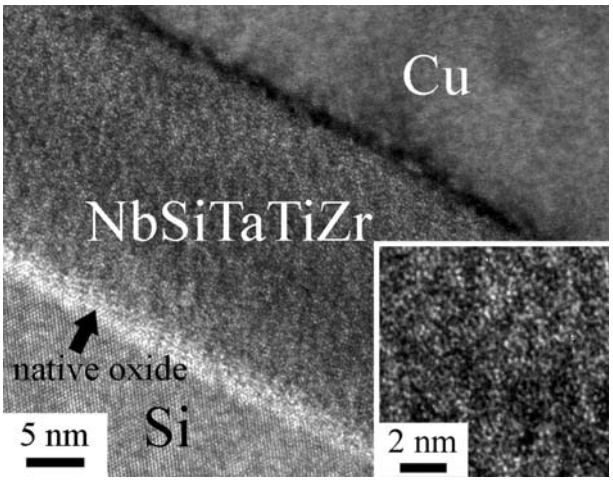

Figure 4. TEM image of the Cu/NbSiTaTiZr/Si test structure after 800°C annealing. Inset shows the high resolution image of the NbSiTaTiZr barrier.

deterioration has occurred even in regions without the appearance of silicides.

Fig. 4 shows the cross-sectional TEM images of the test structure after annealing at 800°C. Three distinct layers with sharp interfaces can be observed. This means that the barrier is effective and there is no interdiffusion. Note that the single-crystal lattice image of the Si substrate remains intact, and no silicidation reaction is observed. Therefore, NbSiTaTiZr indeed remains its chemical stability against Si to 800°C. Additionally, from the inset of Fig. 4, which shows the high-resolution TEM image of the barrier, we can see that NbSiTaTiZr HEA retains its amorphous nature after annealing at 800°C. We note that virtually all known conventional amorphous metals, even those with high glass forming ability, crystallizes at 550°C.[31–33] Therefore, the extremely high structural stability of NbSiTaTiZr barrier is unique and striking.

As stated previously, numerous Cu_3Si crystals already form on the sample surface after annealing at 850°C. However, no silicide is observed on the majority of the sample surface, which is still covered by the remnant Cu film. Cross sectional TEM observation was carried out in these areas to see if Cu-Si interdiffusion has taken place. Fig. 5a

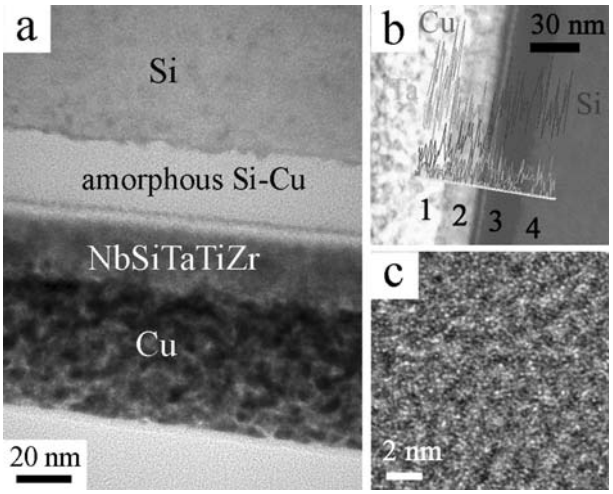

Figure 5. (a) TEM image of the Cu/NbSiTaTiZr/Si test structure after 850°C annealing. (b) EDS linescan profiles superimposed on the STEM image of the 850°C-annealed sample. Layers 1, 2, 3, and 4 are the Cu film, the barrier, the amorphous Si-Cu layer, and the Si substrate, respectively. (c) High resolution image of the Si-Cu amorphous layer in (a).

Table I. Composition of each layer in Fig. 5c by EDS (in at.%). The small negative value of Ti in layer 4 given by the software is a systematic error that occurs when the concentration of the element is too small.

	Cu	Si	Nb	Ta	Ti	Zr
Layer 1	74.0	15.8	1.5	4.2	3.3	1.2
Layer 2	39.0	24.2	9.3	12.6	6.2	8.6
Layer 3	7.2	91.9	0.2	0.4	0.1	0.2
Layer 4	5.4	94.2	0.1	0.2	−0.2	0.2

shows the cross-sectional image of these areas. Between Cu and Si, there now exist two uniform layers, both with a thickness of 20 nm (layers 2 and 3 in Fig. 5b). EDS results (Table I) reveals that layer 2 is the NbSiTaTiZr barrier and layer 3 has a composition of 91.9 at.% Si and 7.2 at.% Cu. High resolution image of layer 3 shows that it has an amorphous structure (Fig. 5c). Formation of such amorphous layer is typical of the preliminary stage of Cu diffusion into Si,[34,35] and is closely related to the solid-state amorphization phenomenon, as has been well studied in various metal/Si systems.[16,36–38] Formation of such amorphous Si-Cu layer indicates that the barrier has failed to prevent the interdiffusion of Cu and Si at 850°C. Indeed, line-scan results in Fig. 5b reveal that Cu and Si have diffused across the barrier. EDS result of the Cu film (layer 1) also shows apparent Si invasion. Therefore, global failure of the barrier has occurred due to the interdiffusion of Cu and Si at 850°C.

The effective temperature of NbSiTaTiZr (800°C) is significantly higher than that of conventional metal barriers (550–650°C). In fact, such temperature is comparable to many ceramic barriers. For example, the effective temperatures of TaN, ZrB_2 and TaSiN barriers with 20–30 nm thickness are reported to be 750, 750, and 800°C, respectively.[15,39,40] The fact that both NbSiTaTiZr and AlCrRuTaTiZr (ref. 28) reach ceramics-like stability demonstrates that HEAs can have great potential in areas where high thermal stability is required, provided that the composition is carefully designed.

Discussion

Structural stability of NbSiTaTiZr.— The superior performance of the NbSiTaTiZr HEA should be attributed to its excellent structural and chemical stabilities. As stated in the introduction, grain boundaries are fast diffusion pathways for Cu.[2] The stability of the amorphous barrier structure is therefore crucial. The exceptional stability of the amorphous structure in NbSiTaTiZr can be explained with the following three factors. The first factor is the low driving force for NbSiTaTiZr to crystallize into individual intermetallic compounds. The unique design of the alloy effectively reduces this tendency. The driving force can be estimated by comparing the free energy difference between solid solution and compound states. The formation energy (ΔG) of NbSiTaTiZr alloy at temperature T from its elemental state can be expressed as:

$$\Delta G = \Delta H - T\Delta S \quad [1]$$

where ΔH and ΔS are the formation enthalpy and formation entropy of the alloy, respectively. The formation enthalpy (ΔH) of 1 mole NbSiTaTiZr atoms (0.2 mole of each element) can be estimated using the following equation:[41]

$$\Delta H = 4\sum_{\substack{i,j=1\\ i>j}}^{n} \Delta H_{ij}^{mix} c_i c_j \quad [2]$$

where n is the total number of elements in the alloy, c_i and c_j are the concentration of the i-th and j-th element, and ΔH_{ij}^{mix} is the heat of mixing for the i-th and j-th element, respectively. The values of ΔH_{ij}^{mix} are listed in Table II.[42] Thus, the formation enthalpy (ΔH) is 29.4 kJ (mole of atoms)$^{-1}$. The formation entropy comes mainly

Table II. Values of ΔH_{mix} [kJ (mole of atoms)$^{-1}$] for all possible atomic pairs in the NbSiTaTiZr alloy.[42]

	Nb	Si	Ta	Ti	Zr
Nb	–	−39	0	2	4
Si		–	−39	−49	−67
Ta			–	1	3
Ti				–	0
Zr					–

from configurational entropy,[18,19] which can be calculated based on Boltzmann's entropy formula:

$$\Delta S_{conf} = -k \ln \omega \quad [3]$$

where k is Boltzmann's constant and ω is the number of ways of mixing. Therefore, the configurational entropy of mixing in an equimolar quinary alloy is Rln5 according to Equation 3, where R is the gas constant. If we set the temperature to 800°C, entropy change contributes −14.36 kJ/mole and thus the formation energy of NbSiTaTiZr random solid solution can be calculated from Equation 1 to be −43.80 kJ (mole of atoms)$^{-1}$.

Now, we consider the formation energy when the alloy crystallizes into individual compounds. By inspecting Table II it can be seen that except Si, other elements in this alloy have zero or positive enthalpy of mixing with respect to each other. This means that Nb, Ta, Ti, Zr will not react with each other. Therefore, calculating the lowest possible free energy when NbSiTaTiZr crystallizes into compounds becomes easy – simply consider the set of silicides that will yield the largest negative formation enthalpy. Since Si content is only 20 at. %, not all metallic elements will react with Si. Moreover, Zr- and Ti-silicides have apparently larger negative formation enthalpy than silicides of Nb and Ta.[43] Therefore, we can consider only Zr- and Ti-silicides. In such Si-deficient situation, largest negative formation enthalpy will be achieved with silicides that leads to as low formation enthalpy as possible with as little Si as possible. Therefore, we calculate the "formation enthalpy per mole Si atoms" of each silicide by dividing the formation enthalpy of a silicide by the amount of Si atoms (in mole) in it. For example, the formation enthalpy of Ti_5Si_3 shall be divided by 3 because each mole of Ti_5Si_3 contains 3 moles of Si atoms. Table III lists the formation enthalpy and the formation enthalpy per mole Si atoms of Zr- and Ti-silicides.[43–45] It can be seen that the higher the metal-to-silicon ratio, the higher the formation enthalpy per mole Si. Note that although Zr_3Si and Ti_3Si have large formation enthalpy per mole Si atoms, the amount of these silicides is limited due to insufficient Zr and Ti (also shown in Table III). Therefore, the lowest free energy state will be achieved when 1 mole atoms of NbSiTaTiZr alloy (0.2 mole of each element) crystallizes into 0.033 mole of Ti_5Si_3 and 0.1 mole of Zr_2Si, with a formation enthalpy of −41.07 kJ (mole of atoms)$^{-1}$. Since compounds have negligible configurational entropy due to their ordered structure, the entropy of the alloy will come from the unreacted atoms: 0.2 mole of Nb and Ta, plus 0.033 mole of Ti. Let's assume in the best case where all unreacted atoms form a random solid solution, which gives us an entropy of 3.255 J (K mole)$^{-1}$. Therefore, at 800°C, the lowest formation energy achievable when NbSiTaTiZr alloy crystallizes into individual silicides can be calculated from Equation 1 to be −44.56 kJ (mole of atoms)$^{-1}$. Comparing the free energy difference between solid solution and crystallized compound state, it is seen that the driving force for crystallization into individual compounds is only −0.76 kJ (mole of atoms)$^{-1}$. This clearly explains why NbSiTaTiZr does not crystallize into individual compounds even at 800°C.

Table IV. Formation enthalpy values of the most Si-rich silicide for each metal in NbSiTaTiZr alloy.[43,47]

Element	Nb	Ta	Ti	Zr
Most Si-rich compound	$NbSi_2$	$TaSi_2$	$TiSi_2$	$ZrSi_2$
ΔH (kJ mole^{-1})	−161.1	−116.4	−171.0	−153.9

The second factor that contributes to the stability of the amorphous structure is the severe lattice distortion in crystalline HEAs. In contrast to the first factor, this factor hinders the direct crystallization of the alloy without compositional redistribution. The severe lattice distortion in HEAs results from the large atomic size differences among the various (at least five, by definition of HEA) principal elements. The lattice strain energies produced by this distortion can markedly raise the overall free energy of the crystalline structure. In contrast, strain energy arising from lattice distortion can basically be regarded as zero in an amorphous structure since there is no lattice framework. Thus, the free-energy difference between crystalline and amorphous structures is largely reduced, and a significantly lower driving force for crystallization is expected. The third factor is the reduced diffusion kinetics in NbSiTaTiZr, which comes from the efficient packing in the alloy. In NbSiTaTiZr, large size differences exist. For example, Si is 18.2% smaller than the average atomic size (143 pm), while Zr is 11.9% larger than the average. It has been pointed out that amorphous metals whose constituent elements show large size differences have a higher atomic packing density.[46] This means there will be less free volume in the amorphous structure, making atomic rearrangement more difficult. Such mechanism has been found to be an important reason for the stabilization of amorphous alloys.[46] Moreover, most elements in the alloy have high melting points. This would also lead to a slower diffusion rate within the alloy.

Table III. Formation enthalpy (ΔH) and formation enthalpy per mole Si atoms of various Ti- and Zr-silicides. Limiting element and the maximum amount of silicide that could be formed when 1 mole atoms of NbSiTaTiZr alloy crystallizes are also listed.

Element	Silicide	ΔH (kJ/mol)	ΔH per mole Si atoms (kJ/mol Si atoms)	Limiting element	Max. amount possible (mole)
Ti	Ti_3Si	−200.00	−200.00	Ti	0.067
	Ti_2Si	−175.05	−175.05	Ti	0.100
	Ti_5Si_3	−607.60	−202.53	Ti	0.120
	Ti_5Si_4	−697.77	−174.44	Ti	0.160
	TiSi	−155.06	−155.06	Ti and Si	0.200
	$TiSi_2$	−171.00	−85.50	Si	0.050
Zr	Zr_3Si	−217.36	−217.36	Zr	0.067
	Zr_2Si	−208.16	−208.16	Zr	0.100
	Zr_3Si_2	−384.56	−192.28	Zr	0.133
	Zr_5Si_3	−575.17	−191.72	Zr	0.120
	ZrSi	−154.66	−154.66	Zr and Si	0.200
	$ZrSi_2$	−153.90	−76.95	Si	0.050

Chemical stability of NbSiTaTiZr.— The better chemical stability against reacting with Si substrate is again a result of the lower free energy state of NbSiTaTiZr alloy relative to that of simple alloy systems. A lower energy state means the alloy will be more stable, and will have a smaller driving force for silicidation reaction. This can be understood by comparing the driving force for silicidation of unalloyed NbSiTaTiZr (five pure elements) and that of alloyed NbSiTaTiZr. Table IV lists the formation energies of Nb-, Ta-, Ti- and Zr-silicides. Only the most Si-rich compound is listed because there is basically unlimited amount of Si from the substrate. Therefore, when unalloyed NbSiTaTiZr reacts with Si to form silicides, the formation enthalpy is -120.5 kJ (mole of atoms)$^{-1}$ (i.e., the driving force is -120.5 kJ mole^{-1}). However, the driving force for silicidation of the alloyed NbSiTaTiZr is only -76.7 kJ (mole of atoms)$^{-1}$ because its formation energy is -43.80 kJ (mole of atoms)$^{-1}$ as calculated previously. This means the driving force for the alloy is 36% lower than that of pure elements! This significantly lower driving force explains why NbSiTaTiZr has much better resistance to silicidation with Si substrate than conventional metal barriers.

Conclusions

In summary, we demonstrate a 20-nm-thick NbSiTaTiZr diffusion barrier which is capable of preventing the interdiffusion and reaction between Cu and Si at 800°C for 30 min. Such effective temperature is comparable to many ceramic barriers. The superior performance of NbSiTaTiZr is owing to the higher structural stability (of its amorphous structure) and higher chemical stability (against reaction with Si substrate) as compared to conventional metal barriers. The structural stability comes from the low driving force of crystallizing into compounds, the severe lattice strain, and the slow diffusion kinetics in the alloy. The chemical stability comes from its lower free energy level.

Acknowledgments

This work is supported by the National Science Council of Taiwan under Grant No. 952120M007004 and National Tsing Hua University under Grant No. 97N2558E1.

References

1. *International Technology Roadmap for Semiconductors, 2009 Edition*. Available from: http://www.itrs.net/Links/2009ITRS/Home2009.htm.
2. A. E. Kaloyeros and E. Eisenbraun, *Annu. Rev. Mater. Sci*., **30**, 363 (2000).
3. A. A. Istratov and E. R. Weber, *J. Electrochem. Soc*., **149**, G21 (2002).
4. M. A. Nicolet, *Thin Solid Films*, **52**, 415 (1978).
5. H. Kim, Y. Naito, T. Koseki, T. Ohba, T. Ohta, Y. Kojima, H. Sato, and Y. Shimogaki, *Jpn. J. Appl. Phys*., **45**, 2497 (2006).
6. H. Kim, T. Koseki, T. Ohba, T. Ohta, Y. Kojima, H. Sato, and Y. Shimogaki, *J. Electrochem. Soc*., **152**, G594 (2005).
7. K. Abe and H. Onoda, *J. Vac. Sci. Technol., B*, **21**, 1161 (2003).
8. M. W. Lane, C. E. Murray, F. R. McFeely, P. M. Vereecken, and R. Rosenberg, *Appl. Phys. Lett*., **83**, 2330 (2003).
9. O. Chyan, T. N. Arunagiri, and T. Ponnuswamy, *J. Electrochem. Soc*., **150**, C347 (2003).
10. T. N. Arunagiri, Y. Zhang, O. Chyan, M. El-Bouanani, M. J. Kim, K. H. Chen, C. T. Wu, and L. C. Chen, *Appl. Phys. Lett*., **86**, 083104 (2005).
11. E. Kolawa, J. S. Chen, J. S. Reid, P. J. Pokela, and M. A. Nicolet, *J. Appl. Phys*., **70**, 1369 (1991).
12. K. M. Chang, T. H. Yeh, I. C. Deng, and C. W. Shih, *J. Appl. Phys*., **82**, 1469 (1997).
13. J. S. Fang, T. P. Hsu, and G. S. Chen, *J. Electron. Mater.*, **33**, 1176 (2004).
14. M. Takeyama, A. Noya, and T. Fukuda, *J. Vac. Sci. Technol., A*, **15**, 415 (1997).
15. M. T. Wang, Y. C. Lin, and M. C. Chen, *J. Electrochem. Soc*., **145**, 2538 (1998).
16. J. Y. Cheng and L. J. Chen, *J. Appl. Phys*., **69**, 2161 (1991).
17. J. C. Chuang, S. L. Tu, and M. C. Chen, *Thin Solid Films*, **346**, 299 (1999).
18. J. W. Yeh, S. K. Chen, S. J. Lin, J. Y. Gan, T. S. Chin, T. T. Shun, C. H. Tsau, and S. Y. Chang, *Adv. Eng. Mater.*, **6**, 299 (2004).
19. J. W. Yeh, *Ann. Chim. - Sci. Mat*., **31**, 633 (2006).
20. Y. Y. Chen, U. T. Hong, J. W. Yeh, and H. C. Shih, *Appl. Phys. Lett*., **87**, 261918 (2005).
21. C. H. Lai, S. J. Lin, J. W. Yeh, and S. Y. Chang, *Surf. Coat. Technol*., **201**, 3275 (2006).
22. Y. J. Zhou, Y. Zhang, Y. L. Wang, and G. L. Chen, *Mater. Sci. Eng. A-Struct. Mater. Prop. Microstruct. Process*., **454**, 260–265 (2007).
23. P. K. Huang and J. W. Yeh, *Scripta Mater.*, **62**, 105 (2010).
24. Y. Y. Chen, U. T. Hong, J. W. Yeh, and H. C. Shih, *Scripta Mater.*, **54**, 1997 (2006).
25. M. H. Tsai, C. W. Wang, C. H. Lai, J. W. Yeh, and J. Y. Gan, *Appl. Phys. Lett*., **92**, 052109 (2008).
26. S. Y. Chang and D. S. Chen, *Appl. Phys. Lett*., **94**, 231909 (2009).
27. S. Y. Chang and D. S. Chen, *Mater. Chem. Phys*., **125**, 5 (2011).
28. M. H. Tsai, J. W. Yeh, and J. Y. Gan, *Thin Solid Films*, **516**, 5527 (2008).
29. S. Y. Chang, C. Y. Wang, M. K. Chen, and C. E. Li, *J. Alloys Compd*., **509**, L85 (2011).
30. T. H. Yang, R. T. Huang, C. A. Wu, F. R. Chen, J. Y. Gan, J. W. Yeh, and J. Narayan, *Appl. Phys. Lett*., **95**, 241905 (2009).
31. W. H. Wang, C. Dong, and C. H. Shek, *Mater. Sci. Eng. R-Rep*., **44**, 45 (2004).
32. G. Duan, A. Wiest, M. L. Lind, J. Li, W. K. Rhim, and W. L. Johnson, *Adv. Mater.*, **19**, 4272 (2007).
33. Z. P. Lu and C. T. Liu, *Acta Mater.*, **50**, 3501 (2002).
34. J. Echigoya, H. Enoki, T. Satoh, T. Waki, T. Ohmi, M. Otsuki, and T. Shibata, *Appl. Surf. Sci*., **56-8**, 463 (1992).
35. J. Echigoya, T. Satoh, and T. Ohmi, *Acta Metall. Mater.*, **41**, 229 (1993).
36. H. C. Cheng, T. R. Yew, and L. J. Chen, *J. Appl. Phys*., **57**, 5246 (1985).
37. W. Lur and L. J. Chen, *Appl. Phys. Lett*., **54**, 1217 (1989).
38. J. Y. Cheng and L. J. Chen, *Appl. Phys. Lett*., **56**, 457 (1990).
39. J. W. Sung, D. M. Goedde, G. S. Girolami, and J. R. Abelson, *J. Appl. Phys*., **91**, 3904 (2002).
40. Y. J. Lee, B. S. Suh, S. K. Rha, and C. O. Park, *Thin Solid Films*, **320**, 141 (1998).
41. A. Takeuchi and A. Inoue, *Mater. Trans., JIM*, **41**(11), 1372–1378 (2000).
42. F. R. de Boer, R. Boom, W. C. M. Mattens, A. R. Miedema, and A. K. Niessen, *Cohesion in Metals: Transition Metal Alloys*, Elsevier Science Publishers B.V., Amsterdam, Netherlands (1988).
43. M. E. Schlesinger, *Chemical Reviews*, **90**, 607 (1990).
44. R. Hultgren, P. D. Desai, D. T. Hawkins, M. Gleiser, and K. K. Kelley, *Selected values of the thermodynamic properties of binary alloys*, Amer. Soc. Metals, Metals Park, Ohio, USA (1973).
45. H. J. Seifert, H. L. Lukas, and G. Petzow, *Z. Metallkd.*, **87**(1), 2–13 (1996).
46. A. Inoue, *Acta Mater.*, **48**, 279 (2000).
47. S. V. Meschel and O. J. Kleppa, *J. Alloys Compd*., **274**, 193 (1998).